

Free-space optical delay interferometer with tunable delay and phase

Jingshi Li,^{1,*} Kai Worms,¹ Ruediger Maestle,² David Hillerkuss,¹ Wolfgang Freude,¹ and Juerg Leuthold¹

¹Institute of Photonics and Quantum Electronics, Karlsruhe Institute of Technology, Karlsruhe, D-76131, Germany

²Agilent Technologies, Boeblingen, Germany

*jingshi.li@kit.edu

Abstract: A free-space optical delay interferometer (DI) featuring a continuously tunable time delay, polarization insensitive operation with high extinction ratios and accurate phase and time delay monitoring scheme is reported. The polarization dependence is actively mitigated by adjusting a birefringent liquid-crystal device. The DI has been tested for reception of D(m)PSK signals.

©2011 Optical Society of America

OCIS codes: (060.5060) Phase modulation; (120.3180) Interferometry.

References and links

1. R. A. Griffin, R. I. Johnstone, R. G. Walker, J. Hall, S. D. Wadsworth, K. Berry, A. C. Carter, M. J. Wale, J. Hughes, P. A. Jerram, and N. J. Parsons, "10 Gb/s optical differential quadrature phase shift key (DQPSK) transmission using GaAs/AlGaAs integration," in *Proc. Optical Fiber Communication Conference (OFC'02)*, (Anaheim, CA, USA, 2002), Postdeadline Paper FD6.
2. A. H. Gnauck, G. Raybon, S. Chandrasekhar, J. Leuthold, C. Doerr, L. Stulz, A. Agarwal, S. Banerjee, D. Grosz, S. Hunsche, A. Kung, A. Marhelyuk, D. Maywar, M. Movassaghi, X. Liu, C. Xu, X. Wei, and D. M. Gill, "2.5 Tb/s (64'42.7 Gb/s) transmission over 40'100 km NZDSF using RZ-DPSK format and all-Raman-amplified spans," in *Proc. Optical Fiber Communication Conference (OFC'02)*, (Anaheim, CA, USA, 2002), Postdeadline Paper PD FC2.
3. N. Kikuchi, K. Mandai, S. Sasaki, and K. Sekine, "Proposal and first experimental demonstration of digital incoherent optical field detector for chromatic dispersion compensation," in *Proc. of European Conference on Optical Communication (ECOC'06)*, (Cannes, France, 2006), paper Th444.
4. X. Liu, S. Chandrasekhar, and A. Leven, "Digital self-coherent detection," *Opt. Express* **16**(2), 792–803 (2008).
5. J. Li, K. Worms, P. Vorreau, D. Hillerkuss, A. Ludwig, R. Maestle, S. Schuele, U. Hollenbach, J. Mohr, W. Freude, and J. Leuthold, "Optical vector signal analyzer based on differential direct detection," in *Proc. of IEEE Photonics Society (LEOS) 2009*, (Belek-Antalya, Turkey, 2009), Paper TuA4.
6. J. Leuthold, B. Mikkelsen, G. Raybon, C. H. Joyner, J. L. Pleumeekers, B. I. Miller, K. Dreyer, and R. Behringer, "All-optical wavelength conversion between 10 and 100 Gb/s with SOA delayed-interference configuration," *Opt. Quantum Electron.* **33**(7/10), 939–952 (2001).
7. S. Sygletos, R. Bonk, T. Vallaitis, A. Marculescu, P. Vorreau, J. Li, R. Brenot, F. Lelarge, G.-H. Duan, W. Freude, and J. Leuthold, "Filter assisted wavelength conversion with quantum-dot SOAs," *J. Lightwave Technol.* **28**(6), 882–897 (2010).
8. D. Hillerkuss, M. Winter, M. Teschke, A. Marculescu, J. Li, G. Sigurdsson, K. Worms, S. Ben Ezra, N. Narkiss, W. Freude, and J. Leuthold, "Simple all-optical FFT scheme enabling Tbit/s real-time signal processing," *Opt. Express* **18**(9 Issue 9), 9324–9340 (2010).
9. G. Bosco and P. Poggiolini, "On the joint effect of receiver impairments on direct-detection DQPSK systems," *J. Lightwave Technol.* **24**(3), 1323–1333 (2006).
10. B. Mikkelsen, C. Rasmussen, P. Mamyshev, and F. Liu, "Partial DPSK with excellent filter tolerance and OSNR sensitivity," *Electron. Lett.* **42**(23), 1363–1364 (2006).
11. Y. Nasu, K. Hattori, T. Saida, Y. Hashizume, and Y. Sakamaki, "Silica-based adaptive-delay DPSK demodulator with a cascaded Mach-Zehnder interferometer configuration," in *Proc. European Conference on Optical Communication (ECOC), 2010*, (Torino, Italy, 2010) paper We.8.E.5.
12. L. Christen, Y. K. Lize, S. Nuccio, L. Paraschis, and A. E. Willner, "Experimental demonstration of reduced complexity 43-Gb/s RZ-DQPSK rate-tunable receiver," *IEEE Photon. Technol. Lett.* **20**(13), 1166–1168 (2008).
13. H. Kawakami, E. Yoshida, Y. Miyamoto, and M. Oguma, "Analysing the penalty induced by PD of MZI in DQPSK receiver using novel measuring technique," *Electron. Lett.* **43**(2), 121–122 (2007).
14. H. Kawakami, E. Yoshida, Y. Miyamoto, M. Oguma, and T. Itoh, "Simple phase offset monitoring technique for 43 Gbit/s optical DQPSK receiver," *Electron. Lett.* **44**(6), 437–438 (2008).

15. Z. Tao, A. Isomura, T. Hoshida, and J. C. Rasmussen, "Dither-free, accurate, and robust phase offset monitor and control method for optical DQPSK demodulator" in *Proc. European Conference on Optical Communication (ECOC), 2007*, (Berlin, Germany, 2007) paper Mo.3.D.5.
16. L. Rovati, U. Minoni, M. Bonardi, and F. Docchio, "Absolute distance measurement using comb-spectrum interferometry," *J. Opt.* **29**(3), 121–127 (1998).
17. A. Cabral and J. Rebordao, "Accuracy of frequency-sweeping interferometry for absolute distance metrology," *Opt. Eng.* **46**, 073602 (2007).
18. S. Schüle, U. Hollenbach, J. Mohr, J. Li, P. Vorreau, A. Efremov, J. Leuthold, and S. Schonhardt, "Modular integration of microactuators and micro-optical benches," in *Proc. of SPIE Conference on Micro-Optics*, (Strasbourg, France, April 2008) vol. 6992, pp. 699202–699202–12 (2008).
19. J. Li, K. Worms, D. Hillerkuss, B. Richter, R. Maestle, W. Freude, and J. Leuthold, "Tunable free space optical delay interferometer for demodulation of differential phase shift keying signals," in *Proc. Optical Fiber Communication Conference (OFC 2010)*, (San Diego, Ca, USA, 2010), paper JWA24.
20. D. O. Caplan, M. L. Stevens, and J. J. Carney, "High-sensitivity multi-channel single-interferometer DPSK receiver," *Opt. Express* **14**(23), 10984–10989 (2006).
21. A. A. Freschi and J. Frejlich, "Adjustable phase control in stabilized interferometry," *Opt. Lett.* **20**(6), 635–637 (1995).

1. Introduction

Delay interferometers (DIs) are needed to demodulate differential phase shift keying modulation formats, e.g. DBPSK, DQPSK and higher-level formats like D8PSK (for short, D(m)PSK). These formats have various advantages regarding noise, nonlinearities, and dispersion tolerance [1,2]. Recently, DIs have been used to detect the amplitude and optical phase of coherent data signals [3–5]. The main advantage of such a "self-coherent" detection scheme [4] over a real coherent reception is that self-coherent detection does not require an expensive, possibly wideband-tunable local oscillator. Moreover, DIs have also been used as optical filters for all-optical wavelength conversion [6,7]. More recently, DI's have been used as ultrafast optical FFT processing elements enabling FFT processing of a 10 Tbit/s OFDM signal [8].

While delay interferometers have become important for all of the above and many more applications the fabrication of versatile delay interferometers is a challenge to this day. For the above mentioned applications, a versatile DI should feature:

- Tunability in delay time and tunability for phase. In almost any of the above mentioned applications a good reception quality, requires adaption of the time delay to the symbol rate [9]. In again other instances, it is sometimes advantageous to deviate from the one-symbol delay in order to mitigate transmission impairments caused by effects such bandwidth-narrowing by concatenated filters [10]. A DI with a continuously tunable delay would fulfill both requirements. Recently, a DI with adaptive delay has been presented by using cascaded Mach-Zehnder interferometers [11], however this only provides a discrete switching of three delays. A continuously tunable DI has been proposed in [12], where the delay is introduced by passing two orthogonal polarizations through a tunable differential group delay (DGD) element. This scheme, however, requires that the input signal has equal power for both orthogonal polarizations.
- Low polarization-dependent loss (PDL), and especially a low polarization-dependent frequency shift (PDFS), which is of particular importance for demodulating D(m)PSK signals [13]. This is normally achieved by carefully selecting the optical coatings, which should perform for all polarizations alike.
- Accurate monitoring and control of the operating point defining phase and time delay. Phase monitoring with a fixed time delay has been intensively discussed based on RF power monitoring [14] or based on a correlation method [15]. Although the efficiency of both methods has been demonstrated, the techniques are complicated, and they are limited to certain data formats and bitrates. A pilot-tone driven lock-in algorithm can be much more effective in fixing the DI operating point, especially for DQPSK

reception, when a DI pair needs be locked to the desired $\pi/2$ relative phase offset. Sophisticated time delay control techniques can be found in the field of distance metrology [16,17]. A simple solution would be to use a known pilot tone, and to count fringes when tuning the DI.

In this paper we present a polarization-insensitive, continuously tunable free-space optical delay interferometer. Our approach operates over a broad wavelength range.

The paper is organized as follows: We first model an optical delay interferometer mathematically. Then we present an appropriate free-space setup, which provides a calibrated, continuously tunable time delay from 0 ps to 100 ps. We achieve PDFS mitigation by employing a liquid-crystal device to compensate the birefringence within the system. Delay and phase are controlled with the help of a pilot tone. Experimentally, we demodulate DQPSK signals at 11.7 GBd, 28 GBd and 42.7 GBd, present eye diagrams and bit error ratios (BER), and compare the outcome to the results measured with a commercially available DI with fixed delay. In the last section we show that with two additional polarization beam splitters four logic DIs can be folded into one single DI which serves as a tunable polarization division multiplexing (PDM) receiver for polarization multiplexed D(m)PSK signals.

2. DI modeling

A schematic DI layout is shown in Fig. 1. It consists of two couplers and two optical paths of different length. The upper path has a time delay of ΔT compared to the lower path. The input electrical fields $E_{in,1}$ and $E_{in,2}$ are split by the first coupler (S_I), then experience two different optical paths, and are then combined at the second coupler (S_{II}), where two output fields $E_{out,1}$ and $E_{out,2}$ are generated.

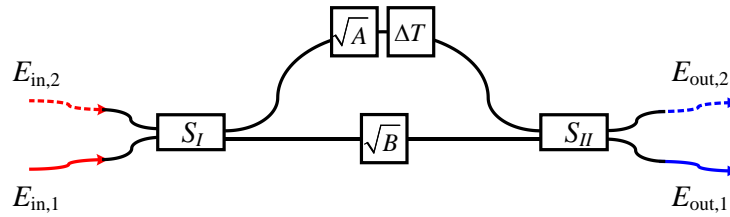


Fig. 1. Schematic of an optical delay interferometer (DI). Inputs ($E_{in,1}$, and $E_{in,2}$) are split by a coupler (S_I) into two paths with A and B as the respective power loss factors. A time delay ΔT is introduced between the two paths. The signals interfere on the other coupler (S_{II}) where two outputs ($E_{out,1}$ and $E_{out,2}$) are generated.

Following [6] we convolve (symbol $*$) the impulse response matrix of the DI with the time-dependent column matrix of input electric fields $E_{in,1,2}$, and find the time-dependent output electric fields $E_{out,1,2}$ (only one polarization is considered):

$$\begin{bmatrix} E_{out,2} \\ E_{out,1} \end{bmatrix} = (S_{II} T S_I)^* \begin{bmatrix} E_{in,2} \\ E_{in,1} \end{bmatrix}, \quad \text{where } S_I = \begin{bmatrix} \sqrt{a(1-s_I)} & j\sqrt{as_I} \exp(j\delta\theta'_{12}) \\ j\sqrt{as_I} \exp(j\delta\theta'_{21}) & \sqrt{a(1-s_I)} \end{bmatrix}, \quad (1)$$

$$T = \begin{bmatrix} \sqrt{A}\delta(t-\Delta T) & 0 \\ 0 & \sqrt{B}\delta(t) \end{bmatrix}, \quad \text{and } S_{II} = \begin{bmatrix} \sqrt{b(1-s_{II})} & j\sqrt{bs_{II}} \exp(j\delta\theta''_{12}) \\ j\sqrt{bs_{II}} \exp(j\delta\theta''_{21}) & \sqrt{b(1-s_{II})} \end{bmatrix}.$$

The matrices S_I and S_{II} in Eq. (1) describe the two couplers, where a phase factor j provides the ideal phase relations between the two output signals, which might be impaired by phase offsets $\delta\theta'_{12}$, $\delta\theta'_{21}$, $\delta\theta''_{12}$, and $\delta\theta''_{21}$. The quantities as_I , $a(1-s_I)$, bs_{II} and $b(1-s_{II})$ are the power splitting ratios of the two couplers in the form of amplitude factors. If $a = 1$ and $b = 1$, the couplers are lossless. The Dirac distributions in matrix T are the impulse responses of the

“long” (upper) and the “short” (lower) arms having a group delay difference ΔT , see Fig. 1. Assuming a monochromatic optical signal with angular frequency $\omega_c = 2\pi f_c$, a change of ΔT introduces a phase offset $-\Delta T\omega_c$ in the upper arm. The quantities $A, B < 1$ are the power loss factors in the two paths.

For a D(m)PSK signal demodulator with only one input to be used, i.e., $E_{in,1} \neq 0, E_{in,2} = 0$, Eq. (1) simplifies to

$$\begin{aligned} E_{out,1}(t) &= \int_{-\infty}^{\infty} \left[-\sqrt{Aabs_I s_{II}} \delta(\tau - \Delta T) \exp\left[j(\delta\theta_{21}'' + \delta\theta_{12}')\right] \right. \\ &\quad \left. + \sqrt{Bab(1-s_I)(1-s_{II})} \delta(\tau) \right] E_{in,1}(t-\tau) d\tau, \\ E_{out,2}(t) &= j \int_{-\infty}^{\infty} \left[\sqrt{Aabs_I(1-s_{II})} \delta(\tau - \Delta T) \exp(j\delta\theta_{12}') \right. \\ &\quad \left. + \sqrt{Babs_{II}(1-s_I)} \delta(\tau) \exp(j\delta\theta_{12}'') \right] E_{in,1}(t-\tau) d\tau. \end{aligned} \quad (2)$$

We can also write Eq. (2) in the frequency domain. We define the Fourier transforms of $E_{out,1,2}(t)$ and $E_{in,1}(t)$ by $\hat{E}_{out,1,2}(f)$ and $\hat{E}_{in,1}(f)$, respectively. The associated transfer functions are $H_{1,2}(f) = \hat{E}_{out,1,2}(f) \exp[j\Phi_{1,2}(f)] = \hat{E}_{out,1,2}(f) / \hat{E}_{in,1}(f)$.

The power transfer function then becomes

$$\begin{aligned} |H_1(f)|^2 &= Bab - [Babs_I + Babs_{II} - (A+B)abs_I s_{II} + 2S \cos(2\pi f \Delta T - \delta\theta_{21}'' - \delta\theta_{12}')], \\ |H_2(f)|^2 &= Babs_{II} + Abs_I - (A+B)abs_I s_{II} + 2S \cos(2\pi f \Delta T + \delta\theta_{12}'' - \delta\theta_{12}'), \\ \text{where } S &= ab\sqrt{ABs_I s_{II}(1-s_I)(1-s_{II})}. \end{aligned} \quad (3)$$

For the associated phases we find:

$$\begin{aligned} \Phi_1(f) &= \tan^{-1} \left[\frac{\sqrt{Aabs_I s_{II}} \sin(2\pi f \Delta T - \delta\theta_{21}'' - \delta\theta_{12}')}{\sqrt{Bab(1-s_I)(1-s_{II})} - \sqrt{Aabs_I s_{II}} \cos(2\pi f \Delta T - \delta\theta_{21}'' - \delta\theta_{12}')} \right], \\ \Phi_2(f) &= \tan^{-1} \left[\frac{\sqrt{Aabs_I(1-s_{II})} \cos(2\pi f \Delta T - \delta\theta_{12}') + \sqrt{Babs_{II}(1-s_I)} \cos(\delta\theta_{12}'')}{\sqrt{Aabs_I(1-s_{II})} \sin(2\pi f \Delta T - \delta\theta_{12}') - \sqrt{Babs_{II}(1-s_I)} \sin(\delta\theta_{12}'')} \right]. \end{aligned} \quad (4)$$

From the frequency dependence of the phase we derive the group delay $\tau_{1,2}(f) = -1/(2\pi) d\Phi_{1,2}(f) / d(f)$,

$$\begin{aligned} \tau_1(f) &= \Delta T \frac{Aabs_I s_{II} - S \cos(2\pi f \Delta T - \delta\theta_{21}'' - \delta\theta_{12}')}{|H_1(f)|^2}, \\ \tau_2(f) &= \Delta T \frac{Aabs_I - [Aabs_I s_{II} - S \cos(2\pi f \Delta T + \delta\theta_{12}'' - \delta\theta_{12}')] }{|H_2(f)|^2}. \end{aligned} \quad (5)$$

For an illustration of Eq. (5) we consider two extreme cases: When $s_I, s_{II} = 0, a, b = 1$, the input field $E_{in,1}$ in Fig. 1 passes exclusively through the lower arm to the output 1. The squared magnitude of the transfer function at the outputs is calculated to be $|H_1(f)|^2 = B, |H_2(f)|^2 = 0$, and the output group delay is $\tau_1(f) = 0$ according to the assumption Eq. (1). When $s_I, s_{II} = 1, a, b = 1$, the input $E_{in,1}$ in Fig. 1 propagates through the upper arm to output 1 without coupling into the lower arm. The squared magnitude of the transfer function at the outputs can be calcu-

lated, $|H_1(f)|^2 = A$, $|H_2(f)|^2 = 0$, and the associated output group delay is $\tau_1(f) = \Delta T$ according to the assumption formulated in Eq. (1).

We describe an ideal DI (no loss, symmetric splitting) by the parameter set

$$A, B, a, b = 1, \quad s_I, s_{II} = \frac{1}{2}, \quad \text{and } \delta\theta_{12}^I, \delta\theta_{21}^I, \delta\theta_{12}^{II}, \delta\theta_{21}^{II} = 0. \quad (6)$$

We define f_0 as a frequency where destructive interference occurs at output 1, and constructive interference at output 2. We plot $|H_{1,2}(f)|^2$ as well as phases $\Phi_{1,2}(f)$ and group delays $\tau_{1,2}(f)$ as a function of the frequency offset from f_0 , blue curves in Fig. 2. The frequency offset is given in units of the free spectral range $\text{FSR} = 1 / \Delta T$. The two outputs have complementary power transfer functions $|H_{1,2}(f)|^2 = 1/2 \cdot (1 \mp \cos(2\pi f \Delta T))$. This leads to an infinite extinction ratio $\text{ER} = (\text{maximum of output 1, 2}) / (\text{minimum of output 2, 1})$, Fig. 2(a). Whenever destructive interference occurs and the transfer function $|H_{1,2}(f)|$ crosses zero, a π -phase shift is observed, Fig. 2(b). These phase jumps result in δ -functions of the group delay, $-\Delta T/2 \cdot \delta(f - N/2\Delta T)$, $N = 0, \pm 1, \pm 2, \pm 3, \dots$, while $\tau_{1,2}(f) = \Delta T/2$ holds at all other frequencies, Fig. 2(c).

In practice, losses and splitting ratios in a DI are not ideal as defined in Eq. (6). As an example we assume 2 dB of losses in one arm, i.e. $A = 0.64$, while all other parameters remain as in Eq. (6). For this case, the quantities $|H_{1,2}(f)|^2$, $\Phi_{1,2}(f)$ and $\tau_{1,2}(f)$ are plotted in Fig. 2 (red curves). In contrast to the ideal case, the red curves have a finite $\text{ER} = 20$ dB, and an additional loss of 0.085 dB. Furthermore, instead of the π -phase jumps, the phase slopes are reduced near the frequency for destructive interference, which results in a finite negative group delay, Fig. 2(c). This behavior is typical for any deviation of A, B, a, b , and s_I, s_{II} from the ideal conditions defined in Eq. (6). Imperfect phase offsets $\delta\theta_{12}^I, \delta\theta_{21}^I, \delta\theta_{12}^{II}, \delta\theta_{21}^{II}$ will introduce a frequency shift of the transfer functions.

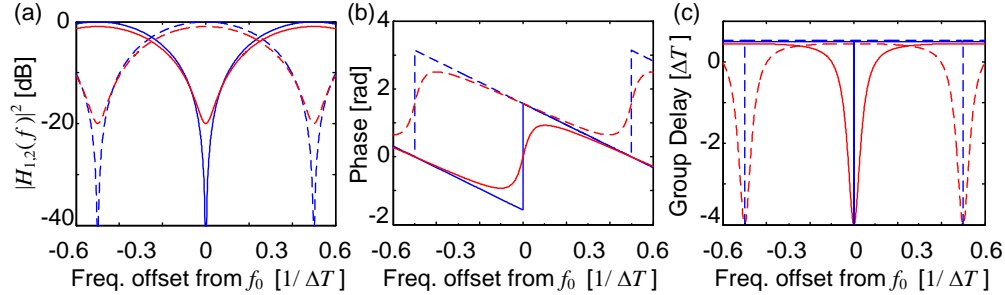


Fig. 2. Transfer function of the DI for different upper-arm power losses $A = 1$ and $A = 0.64$. The case $A = 1$ denotes an ideal DI (blue). The case $A = 0.64$ denotes an imbalanced DI with excess losses in the delayed arm (red). The three plots show (a) the power transfer functions $|H_{1,2}(f)|^2$, (b) the phase response $\Phi_{1,2}(f)$ and (c) the group delay $\tau_{1,2}(f)$ for the constructive output port (dashed lines) and the destructive port (straight lines), respectively.

In the following we use the general model of Eq. (1) for designing a practical implementation of a free-space optics delay interferometer.

3. DI implementation and polarization dependence

DIs typically can be implemented as asymmetric Mach-Zehnder interferometers or as Michelson Interferometers. The two configurations are different though.

A Mach-Zehnder delay interferometer configuration is displayed in Fig. 3(a) [18]. The interferometer is formed by a beamsplitter (BS) and a reflector. The BS splits the collimated input signal (red) in two paths. For changing the optical path length difference, the reflector is mounted on a micro-actuator to create a variable path length with an associated delay ΔT . However we notice that the upper, longer path usually has more loss than the lower path due

to the additional reflector, so that the extinction ratio is degraded. Moreover, the minimum time delay difference ΔT between the two paths is also limited by the fact that the upper optical path is always longer.

Conversely, the Michelson interferometer allows a zero optical path difference and minimal power difference between the signals in both arms, thus providing a (theoretically) infinite large free spectral range (FSR) in combination with a high ER at “Output 1, 2”, see Fig. 3(b) [19].

A prototype has been built as depicted in Fig. 3(c). The signals are coupled with fiber grin lenses into and out of the DI. The dimensions of $85 \times 45 \times 25 \text{ mm}^3$ can be further decreased by using the LIGA technology as in [18]. The actuator used in this setup has a mechanical step size of about 2 nm, which corresponds to a phase offset of about 1° . The mechanical tuning range amounts to 15 mm corresponding to a time delay tuning range of 100 ps. As the actuator responds within milliseconds, the tuning can be performed extremely fast.

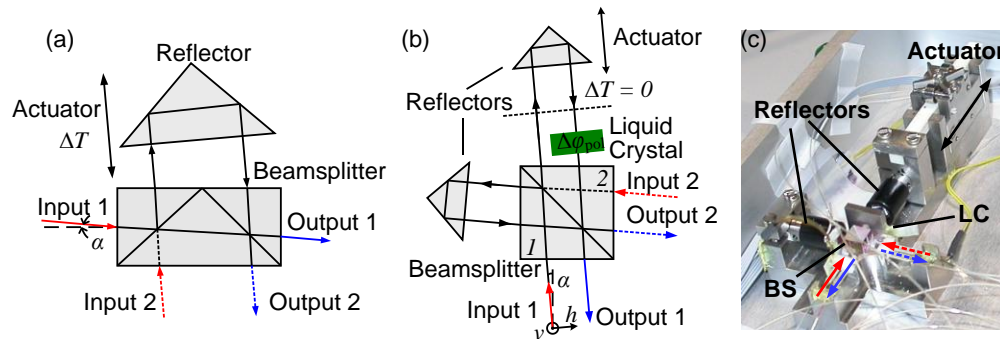


Fig. 3. Practical implementation of DI (a) Schematic of the Mach-Zehnder-DI with two non-polarizing beam splitters (BS) combined in one unit, and one reflector. (b) Schematic of the Michelson DI with single non-polarizing BS and two reflectors. A liquid crystal compensates a polarization dependent frequency shift. (c) Photograph of a prototype of the Michelson DI.

Now we consider an input with two orthogonal polarization states, v and h (“ v ” vertical polarization, and “ h ” horizontal polarization with respect to the incident plane). Because each surface in the system has polarization-dependent transmittivity and reflectivity, the transfer function of the DI is seriously affected by the input signal polarization state. While polarization dependent reflectivity can be minimized by carefully selected coatings, there remains a polarization-dependent phase shift. This phase offset results in a polarization dependent frequency shift (PDFS) of the DI transfer function.

To measure the PDFS of a DI, one could align the input signal parallel to one of two orthogonal (linear) polarizations, and calculate the difference between the respective transfer functions. In practice, because a DI is usually coupled to a standard single mode fiber, the input polarization state for the DI cannot be known. Therefore, we insert a polarizer directly after the input lens and record the spectral response of the DI for horizontal polarization. Then by rotating the polarizer we record the spectral response for a vertical polarization. The spectrally shifted responses are found at “Output 1, 2” and are depicted in Fig. 4(a). Then with the knowledge of the PDFS, we adjust a birefringent element (by voltage tuning a liquid crystal (LC), Fig. 3(b)) for compensating the polarization-induced phase offset. When applying 1 V to the LC, we observe the spectral response in Fig. 4(b), where PDFS has been obviously mitigated as compared to Fig. 4(a).

The PDFS measurement in Fig. 4(c) shows how the birefringence can be undone by detuning the liquid crystal. We have plotted $\Delta\phi_{\text{pol}} = 2\pi$ (PDFS / FSR) against the voltage applied to the liquid crystal. The resolution of the plot is limited by the resolution of the equipment that allowed us to sweep the wavelength with steps of 10 pm only. For a FSR of 200 GHz (1.6 nm) we can resolve a phase difference of 2.2° (0.61% of FSR).

Once the birefringence is undone, it is undone for any delay ΔT as an additional free space does not add to the birefringence. In Fig. 4(a), 4(b) one can notice that the ER = (maximum of output 1, 2) / (minimum of output 1, 2) at “Output 2” for both polarizations is larger than 30 dB. At “Output 1” and for h -polarization the ER is 30 dB as well, however for the v -polarization only 18 dB is measured. This difference is due to the fact transmittivities and reflectivities of the BS coating are slightly polarization dependent. In our case output 2 has an almost ideal extinction ratio because the two beams constructively interfering in the beam splitter and being mapped onto output 2 undergo one reflection and one transmission each. However, the two beams interfering in the BS and being mapped to output 1 undergo two reflections and two transmissions, respectively, which leads to a power imbalance (splitting ratio difference) for the slightest imbalance in the transmission and reflection coefficients of the BS coating. As we discussed above, this will lead to the ER difference between the two outputs at two orthogonal polarizations. As commercially available fixed-delay DIs have typically ER > 18 dB, this prototype has comparable performance. A PDFS < (0.61% of FSR) is also good enough for DQPSK demodulation [9,13].

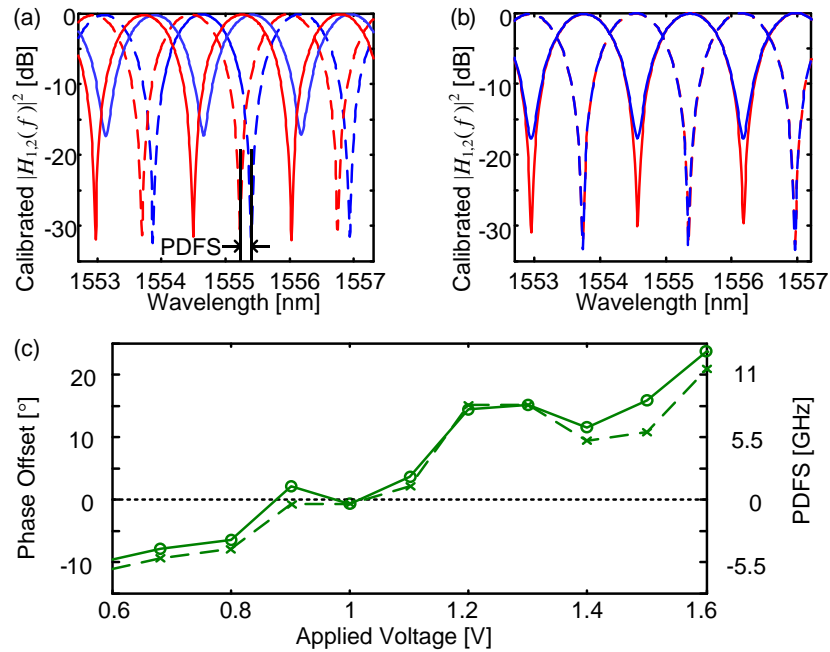


Fig. 4. Spectral response for vertical (blue) and horizontal (red) polarizations. (a) Large PDFS, (b) LC is used to undo birefringence, (c) PDFS of DI for different voltages applied onto the LC (the precision of the measured offset phase is limited by the resolution of the measurement equipment). The plots show the output 2 (dashed lines) and output 1 (straight lines).

Polarization dependent loss (PDL) and differential group delay (DGD) are important as well. Commercial measurement instruments, e.g. Agilent 86038B Photonic Dispersion and Loss Analyzer, Agilent N7788BD Benchtop Optical Component Analyzer, usually provide such data. It is straight forward since PDL and DGD can be derived from the ratio of the transfer functions at orthogonal polarizations,

$$\text{PDL} = \left| 10 \log_{10} \left(\frac{|H_{\text{pol } v}(f)|^2}{|H_{\text{pol } h}(f)|^2} \right) \right|, \quad (7)$$

$$\text{DGD} = \left| \tau_{\text{pol } v}(f) - \tau_{\text{pol } h}(f) \right|.$$

To get an idea of the PDL and DGD to be expected in this device we tune our prototype to minimize PDFS as was done for measuring the data in Fig. 4(c). We record the average squared magnitude of the transfer function for all possible polarizations, find the PDL and detect the DGD as a function of wavelength, Fig. 5(a) and 5(b) (FSR ≈ 42.7 GHz). The peaks in PDL and DGD are due to the different transfer functions for the orthogonal polarizations. When the birefringence control voltage deviates from the optimum operating point, double peaks are observed in the PDL and DGD curves. We then introduce PDFS in a second experiment and consequently find strong PDL and DGD as plotted in Fig. 5(c) and 5(d). The squared magnitude of the transfer function is averaged over all possible polarizations, and therefore the measured ER is small. Thus, one could minimize PDFS by minimizing the PDL and DGD peaks at destructive interference, especially when at the single peaks in Fig. 5(a), 5(b) (upper traces) the PDFS is minimum. The ER of the average squared magnitude of the transfer function for all possible polarizations is maximum when the PDFS is minimum.

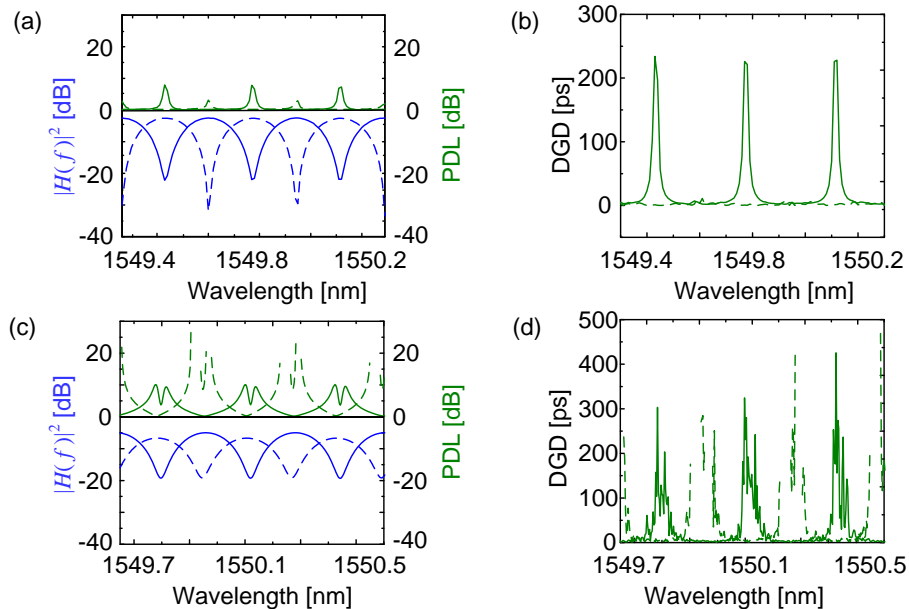


Fig. 5. Measured average squared magnitude of the transfer function for all possible polarizations (blue), of PDL (green), and of DGD (green) at DI output 1 (solid line) and 2 (dashed line); FSR ≈ 42.7 GHz. For minimized PDFS: (a) average loss and PDL. (b) DGD versus wavelength. For large PDFS: (c) average squared magnitude of the transfer function and PDL. (d) DGD versus wavelength.

So far we demonstrated a tunable DI with reduced PDFS. There remains the problem of the inaccurate step size and the hysteresis of the actuator, so we need means for a stable and precise setting of the time delay.

3. Time delay control

In practical application the absolute time delay needs to be controlled and mechanical instabilities need to be mitigated. To this end we design an active feedback control circuit. In Fig. 6(a), the setup of the time delay and phase control is illustrated. A pilot tone at frequency f_p counter-propagates with respect to the communication signal at f_c . Circulators are used for separation of the pilot and signal tone. Because f_p and f_c can be widely different, appropriate filters would also allow a co-propagating arrangement without circulators [20]. For each DI, the pilot tone is detected with a low bandwidth photodiode, sampled for processing in the digital domain and fed to the respective control circuit.

To set the absolute time delay accurately one starts off from a known time delay and then counts the number of constructive and destructive interference fringes m_{\max} and m_{\min} , respectively, when adjusting the delay. The associated change δT of the time delay ΔT can be derived by counting the number of minima and maxima that a signal undergoes when detuning the delay

$$|\delta T| = \frac{m_{\max} + m_{\min}}{2f_p}. \quad (8)$$

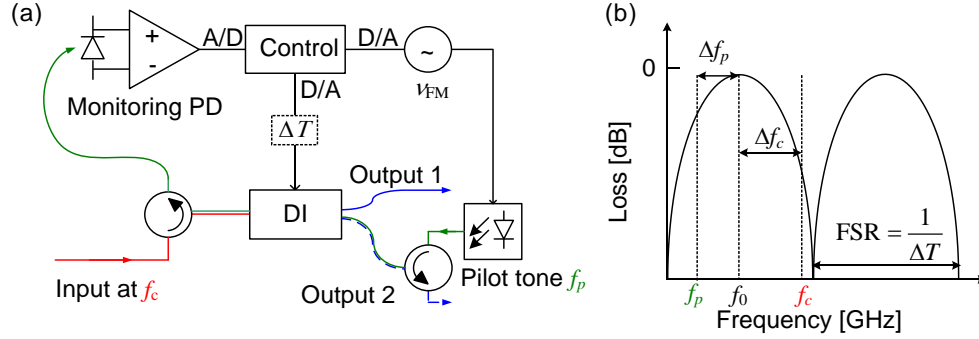


Fig. 6. , Schematic of control circuit (a) Time delay and phase control setup of DI, (b) ideal power transfer function between DI “Input” and “Output 2”.

Since the direction of movement is known, we can estimate the time delay ΔT , and $\Delta T \times c$ (c is the speed of light) is expressed as multiple of the pilot tone wavelength. The remaining delay in distance is less than the wavelength of the pilot tone, which effectively introduces a phase offset to the signal. The remaining phase delay can be found by measuring the power swing of the pilot tone while scanning the delay, and by evaluating the pilot tone power deviation from the average power value at the end of the actuator travel.

For measuring the remaining phase delay more precisely [19] dithering the DI delay may be used [20,21]. However, a mechanical DI dither introduces a deterioration of the transmitted signal data quality. So we decided for dithering the pilot tone frequency f_p harmonically according to $f(t) = f_p + \delta v_d \sin(2\pi v_{FM} t)$ using a frequency deviation δv_d with a modulation frequency v_{FM} . Figure 6(b) shows the power transfer function and denotes its FSR, the DI’s operating frequency f_0 , and the signal carrier frequency f_c . Assuming that the pilot tone is connected to output 2 with f_0 being the frequency with constructive interference in the output, the frequency offset between pilot tone and DI is denoted $\Delta f_p = f_p - f_0$.

The phase monitoring photodiode in Fig. 6(a) produces an output current

$$I_{ac}(t) \propto -J_1(2\pi\delta v_d \Delta T) \sin(2\pi\Delta f_p \Delta T) \sin(2\pi v_{FM} t) + J_2(2\pi\delta v_d \Delta T) \cos(2\pi\Delta f_p \Delta T) \cos(4\pi v_{FM} t) + \dots \quad (9)$$

The symbols $J_{1,2}$ stand for the Bessel functions of order 1 and 2. The amplitudes of $\sin(2\pi v_{FM} t)$ and $\cos(4\pi v_{FM} t)$ can be extracted with a numerical lock-in scheme. ΔT is known with the fringe-counting measurement. Therefore the terms $J_{1,2}(2\pi\delta v_d \Delta T)$ can be estimated with good accuracy, and we calculate Δf_p from the remaining trigonometric terms $\sin(2\pi\Delta f_p \Delta T)$ and $\cos(2\pi\Delta f_p \Delta T)$. With Δf_p and pilot tone f_p known, the frequency f_0 of the transfer function’s maximum is found, which has an offset Δf_c from the carrier frequency f_c . Therefore, based on the known offset Δf_c , a control loop can be set up to fine-tune the delay ΔT for the wanted offset Δf_c , which fixes the phase difference in both arms of the DI. Using the same pilot tone, two DIs in a IQ demodulator can be locked with a defined relative phase offset, i. e. $\pi/2$.

4. Measurement and experiment result

To demonstrate the quality of the tunable delay, we perform experiments with a long a medium and a short delay at 100 ps, 35.7 ps, and 10 ps. The average spectral responses over all possible polarizations, together with PDL versus wavelength are shown in Fig. 7. The plots show from left to right FSRs of 10 GHz (resolution limited), 28 GHz, and 100 GHz. No matter what the delay is the plots show an average ER of more than 20 dB with a minimum PDFS at the two outputs. The PDL around the frequencies of constructive interference are close to zero for all delays.

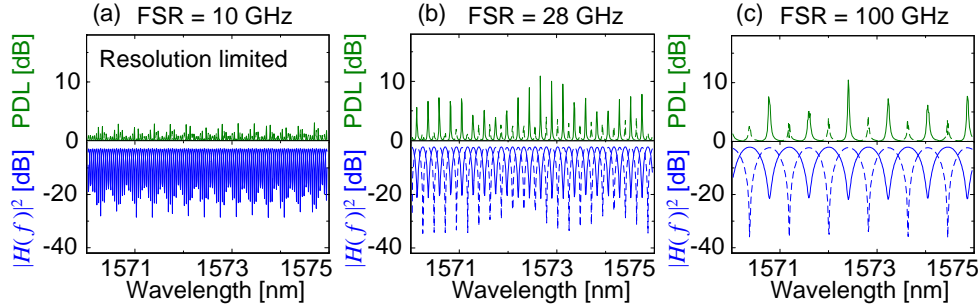


Fig. 7. Average spectral responses (blue) of the two outputs (solid line for output 1 and dashed line for output 2) over all possible polarizations and PDL (green) at FSR = 10 GHz (a), 28 GHz (b) and 100 GHz (c).

We then tested the performance across the spectral range. We performed three measurements with a FSR = 42.7 GHz (delay of 23.4 ps) at different wavelengths, Fig. 8. Similar performances have obtained in each case.

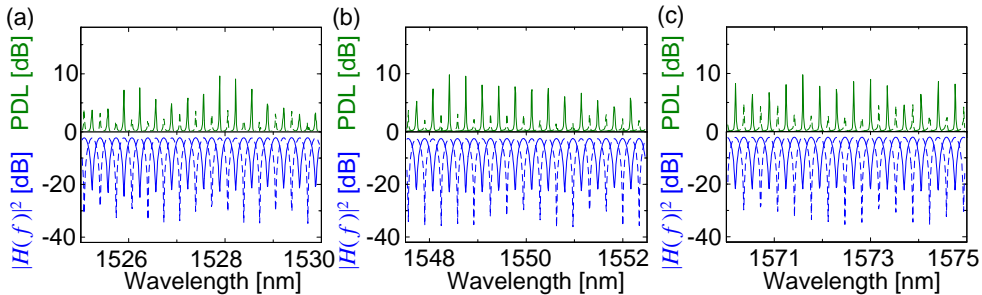


Fig. 8. Average spectral responses (blue) of the two outputs (solid line for output 1 and dashed line for output 2) over all possible polarizations and PDL at wavelength 1525 nm – 1530 nm (a), 1545 nm – 1555 nm (b), and 1570 nm – 1575 nm (c) with FSR = 42.7 GHz.

The accuracy of the absolute delay control algorithms has been tested next. We first set the DI at 700 GHz FSR. We then used a pilot tone at 1550.12 nm to perform the fringe count. The DI is tuned from 700 GHz to 600 GHz and down till 20 GHz, then up to 800 GHz and finally back to 700 GHz. The target value of each of the 40 measurements has been cross-examined with an optical spectrum analyzer (OSA) by connecting the DI input to an ASE source. Figure 9(a) shows the relative deviation between the set FSR and the respective OSA measurement. The maximum deviation is $\pm 0.08\%$, which is mostly limited by the repeatability of the OSA measurement.

We then were interested in the accuracy of setting the DI to a particular phase. For this we modulated the pilot tone with $\nu_{FM} = 60$ Hz and $\delta\nu_d = 2$ GHz and used to scan the phase offset over 360° at FSR = 40 GHz. Results at FSR = 80 GHz are also shown. In Fig. 9(a), the deviations between the set phase offset and the cross-examinations with respect to an OSA are shown. A maximum error of $\sim 2^\circ$ is found. A 6 hours phase deviation measurement is per-

formed with the pilot tone being modulated with $v_{FM} = 30$ Hz and $\delta v_d = 750$ MHz. A phase deviation $< 2^\circ$ and a standard deviation of 0.3° has been measured. The result is shown in Fig. 9(c).

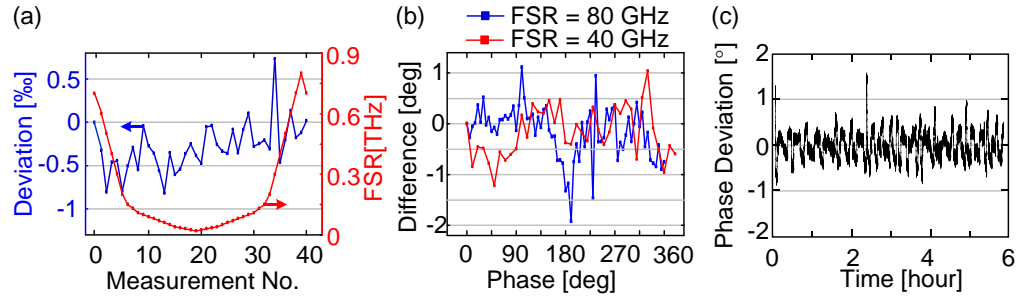


Fig. 9. , The plots (a) the accuracy for setting the absolute time delay (blue curve) when setting the FSR to particular value (red curve) for a measurement cycle between 800 GHz and 20 GHz, (b) the accuracy for setting a particular two delays with FSR = 40 GHz —•— red, FSR = 80 GHz —•— blue for a measurement cycle from 0 to 360 degrees and (c) absolute deviation from set value over time when using the stabilization setup.

The outputs of the DI were then connected to a 50 GHz balanced detector. The balanced receiver was built with a conventional photodiode combined with an inverted photodiode through a RF combiner. Demodulation of NRZ-DQPSK signals was performed at 11.7 GBd, 28 GBd and 42.7 GBd with a DI delay of 1 symbol duration. Eye diagrams of the in-phase channel captured with a DCA are shown in Fig. 10(a). BER measurements were also performed with a PRBS sequence of $2^7 - 1$ at symbol-rates of 28 GBd and 42.7 GBd as depicted in Fig. 10(b). For the two orthogonal polarizations the required received power for fixed BER is almost equal for both symbol-rates with the proposed DI. The performance is comparable with a commercial available DI in the same measurement setup. In Fig. 10(c), similar received power requirement for fixed BER is observed over a broad wavelength range.

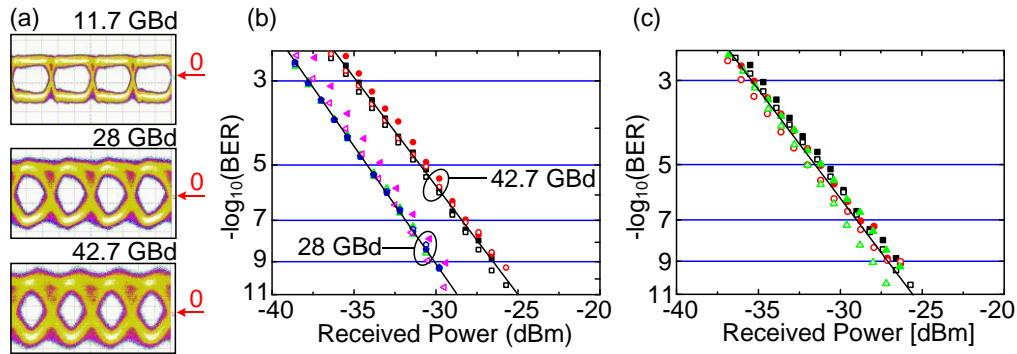


Fig. 10. Measurement results of the proposed DI at various bit rates and comparison with a commercial DI (a) eye diagrams of NRZ-DQPSK I channel at 11.7 GBd, 28 GBd, and 42.7 GBd, (b) BER versus received power at 28 GBd (\blacktriangle , \blacktriangleleft green, for I and Q channels at polarization 1, \bullet , \circ blue for I and Q channels at polarization 2), and 42.7 GBd (\blacksquare , \square black for I and Q channels at polarization 1, \bullet , \circ red for I and Q channels at polarization 2) for orthogonal polarizations of the tunable DI and single polarization of the typical DI (\blacktriangleleft , \blacktriangleright magenta for I and Q channels), and (c) BER versus received power at 42.7 GBd at different wavelengths (\blacksquare , \square black for I and Q channels at 1545.56 nm, \bullet , \circ red at 1550.12 nm, and \blacktriangle , \blacktriangleleft green at 1560.61 nm).

6. Polarization division differential detector

The tunable delay interferometer can be further extended into a polarization division differential detector. We show in a step-by step manner that the four DIs normally used for a polariza-

tion diversity scheme with Inphase (I) and Quadrature (Q) phase detection can be simplified into single DI configuration.

The general concept is first explained on a conventional polarization division differential detector as shown in Fig. 11(a). Its optical front-end includes 4 DIs which have a time delay ΔT that is optimized with respect to the symbol rate of the detected signal. The signal is first split into the two polarization components E_x and E_y (which in general do not correspond to the transmitter's polarization components) by a polarization beam splitter (PBS). Then each polarization is fed into 2 orthogonal DIs ($\pi/2$ relative phase offset) (I- and Q-DIs) and four balanced detectors are used to detect the signal components.

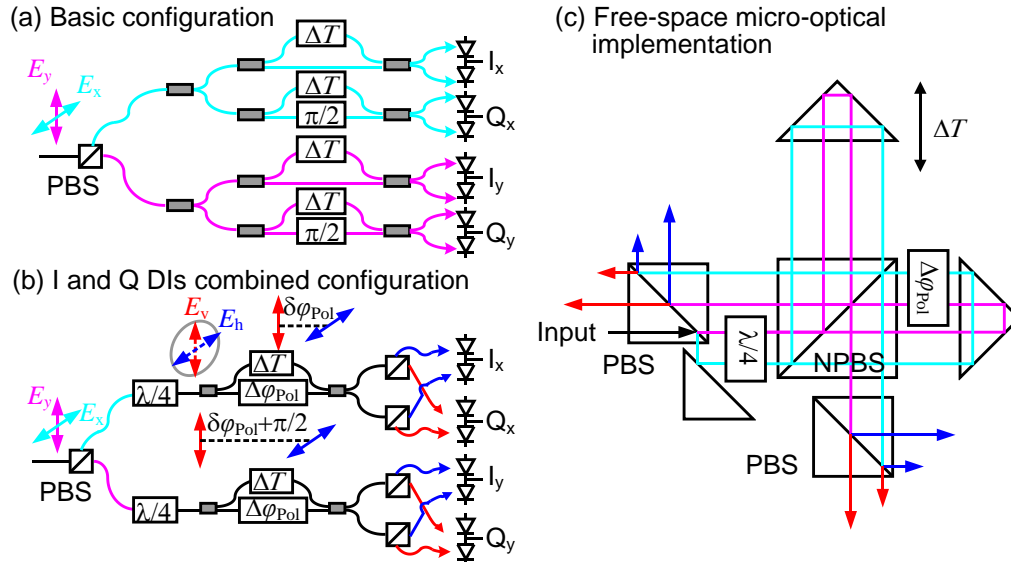


Fig. 11. . Schematics of polarization diversity self-coherent receivers (a) conventional configuration with 4 DIs, (b) I and Q DIs combined configuration with 2 DIs, (c) free-space micro-optical implementation where all elements are folded into 1 DI only.

The DI as described above can be simplified to combine the I- and Q-DIs in a single DI. This novel concept is shown in Fig. 11(b). The scheme works as follows. First a PBS splits off the two polarizations E_x and E_y . Next we would like to determine the I- and Q-phase component of each of the polarizations. So we use quarter-wave plates (QWP) to convert the E_x and E_y components into circular polarizations (which provides us horizontal and vertical fields E_h and E_v . Please note that the real advantage of this scheme is that we have E_h and E_v fields of equal power!). Each circular polarization is then fed into a separate DI. One branch of the DI comprises the time delay and the other branch a birefringent element (e.g. a liquid crystal $\Delta\phi_{Pol}$). The delay may then be set for the h -component to provide the I-phase component. The birefringent element may then be used to set the phase difference in the short branch to $\delta\phi_{Pol} + \pi/2$ resulting in a $\pi/2$ relative phase offset for the v -component with respect to the h -component. The v -component will thus then provide us the Q-phase term. Using PBSs at the DI outputs the E_h and E_v fields can easily be separated and combined into the balanced detectors. Thus we have reduced the number of required DIs to only 2 DIs in this newly proposed configuration.

In Fig. 11(c), we propose an additional reduction of required components in a free space optics implementation. Using a mirror, the two orthogonal polarizations are mapped into the same DI configuration with two beams propagating in parallel sharing the same optical elements. The signals are split and combined with one single NPBS and reflected back by two corner reflectors. One reflector is mounted on a movable actuator that introduces a time delay

ΔT . In the other branch, the birefringent element is set to align the orthogonal relative phase offset between the I and Q-components. Two PBSs (including the one at the input) are used to separate the signals into h and v polarizations. The signals can be coupled into fibers or directly to photodiodes providing electrical signals for further processing. With this novel setup, four logic DIs in a polarization diversity self-coherent detection scheme are folded into one single and compact Michelson delay interferometer structure with one single actuator tuning the time delay.

6. Conclusion

A tunable free-space optical delay interferometer has been modeled and presented. Its delay is controlled with a pilot tone. The maximal time delay is up to 100 ps, which allows a reception of symbol rates $> 10\text{GBd}$. Its PDFS is mitigated by utilizing an adjustable birefringent liquid crystal. A more complex but very compact design for polarization multiplexed D(m)PSK signal detection is also presented.

Acknowledgments

This work is supported by the Agilent University Relation Program, the European Commission's Network of Excellence *EuroFOS* and Karlsruhe School of Optics and Photonics (KSOP).